Journal of Atmospheric and Terrestrial Physics, Vol. 50, Nos 4/5, pp. 467–485, 1988.
Printed in Great Britain.

0021–9169/88 $3.00+ .00
Pergamon Press plc

Scattered power from non-thermal, *F*-region plasma observed by EISCAT—evidence for coherent echoes?

M. LOCKWOOD
Rutherford Appleton Laboratory, Chilton, Didcot, Oxon OX11 0QX, U.K.

K. SUVANTO
Blackett Laboratory, Imperial College, London SW7 2BZ, U.K.

J.-P. ST.-MAURICE, K. KIKUCHI
Center for Atmospheric and Space Sciences, Utah State University, UT 84322–3400, U.S.A.

B. J. I. BROMAGE, D. M. WILLIS, S. R. CROTHERS
Rutherford Appleton Laboratory, Chilton, Didcot, Oxon OX11 0QX, U.K.

H. TODD and S. W. H. COWLEY
Blackett Laboratory, Imperial College, London SW7 2BZ, U.K.

(*Received for publication* 18 *November* 1987)

Abstract—Three rapid, poleward bursts of plasma flow, observed by the U.K.–POLAR EISCAT experiment, are studied in detail. In all three cases the large ion velocities ($> 1\ \mathrm{km\,s^{-1}}$) are shown to drive the ion velocity distribution into a non-Maxwellian form, identified by the characteristic shape of the observed spectra and the fact that analysis of the spectra with the assumption of a Maxwellian distribution leads to excessive rises in apparent ion temperature, and an anticorrelation of apparent electron and ion temperatures. For all three periods the total scattered power is shown to rise with apparent ion temperature by up to 6 dB more than is expected for an isotropic Maxwellian plasma of constant density and by an even larger factor than that expected for non-thermal plasma. The anomalous increases in power are only observed at the lower altitudes (< 300 km). At greater altitudes the rise in power is roughly consistent with that simulated numerically for homogeneous, anisotropic, non-Maxwellian plasma of constant density, viewed using the U.K.–POLAR aspect angle. The spectra at times of anomalously high power are found to be asymmetric, showing an enhancement near the downward Doppler-shifted ion-acoustic frequency. Although it is not possible to eliminate completely rapid plasma density fluctuations as a cause of these power increases, such effects cannot explain the observed spectra and the correlation of power and apparent ion temperature without an unlikely set of coincidences. The observations are made along a beam direction which is as much as 16.5° from orthogonality with the geomagnetic field. Nevertheless, some form of coherent-like echo contamination of the incoherent scatter spectrum is the most satisfactory explanation of these data.

1. INTRODUCTION

Recently, LOCKWOOD *et al.* (1987), MOORCROFT and SCHLEGEL (1988) and WINSER *et al.* (1987) have all reported the effects of non-Maxwellian ion velocity distributions on the spectra of signals received from the ionospheric *F*-region by the EISCAT incoherent scatter radar. These observations were all made when the ion drift was large and with a radar beam at a large angle to the geomagnetic field, in accordance with the theoretical predictions of RAMAN *et al.* (1981), as confirmed by HUBERT (1984).

It has long been known that a supersonic ion gas which collides with a stationary neutral gas will not remain in thermal equilibrium. Hence the plasma in the *F*-region is expected to be driven into non-Maxwellian ion velocity distributions by the combined action of large ion drifts (in the reference frame in which the neutral gas is at rest) and ion–neutral collisions (see review by ST.-MAURICE and SCHUNK, 1979). The exact form of the resulting ion velocity distribution function depends on the nature of the collision process. ST.-MAURICE and SCHUNK (1979) have reviewed their predictions for a variety of simple models of the collision process and BARAKAT *et al.* (1983) have employed Monte Carlo techniques to simulate the effects of a more realistic mixture of resonant charge exchange and polarization elastic scatter interactions. The results show that for sufficiently large bulk ion drifts (greater than the neutral thermal speed), non-Maxwellian or even toroidal ion velocity distributions form.

For non-thermal and/or anisotropic plasma there are a number of definitions of ion temperature. From the second moments of the distributions of ion velocity parallel and perpendicular to the geomagnetic field, the parallel and perpendicular ion temperatures, $T_{\parallel}$ and $T_{\perp}$ respectively, are defined. These values are independent of the shapes of the distributions (see MOORCROFT and SCHLEGEL, 1988). From these two one-dimensional ion temperatures an average, three-dimensional ion temperature T_i is defined by

$$T_i = (T_{\parallel}+2T_{\perp})/3. \quad (1)$$

In addition, a one-dimensional ion temperature for a direction at an angle Φ to the geomagnetic field is given by

$$T_f = T_{\parallel}\cos^2\Phi + T_{\perp}\sin^2\Phi. \quad (2)$$

If the distribution of the ion velocity along the radar line-of-sight (l-o-s) is not Maxwellian and the incoherent scatter spectrum is erroneously analysed with the standard assumption that it is Maxwellian, the derived 'apparent' ion temperature T_{im} can be considerably different to any of the above 'real' ion temperatures (RAMAN et al., 1981). The subscript m denotes the assumption of a Maxwellian distribution. Only in the case of isotropic, Maxwellian plasma are $T_{\perp}$, $T_{\parallel}$, T_f, T_i and T_{im} (to within experimental error) all equal. If the plasma is anisotropic, yet the one-dimensional distribution is still Maxwellian for any Φ (a 'bi-Maxwellian' distribution function), T_{im} will still, to within experimental error, be equal to T_f, but will not in general equal T_i, $T_{\perp}$ or $T_{\parallel}$: T_f varies from $T_{\parallel}$ (for $\Phi = 0$) to $T_{\perp}$ (for $\Phi = 90°$) and equations (1) and (2) show that for $T_{\perp} > T_{\parallel}$ (as expected for large field-perpendicular ion drifts) T_f exceeds T_i if Φ is greater than 54.7°. Lastly, if the l-o-s one-dimensional distribution is not Maxwellian, T_{im} will not equal T_f. In addition, the 'apparent' electron temperature T_{em} will also be in error, but by a smaller factor than T_{im}.

The non-thermal plasma reported by LOCKWOOD et al. (1987) was observed during rapid poleward flow burst events, recorded using the U.K.–POLAR EISCAT experiment (WILLIS et al., 1986). TODD et al. (1986, 1988) have shown that these short-lived (< 5 min) events are consistent with the expected ionospheric signature of flux transfer events at the magnetopause (SOUTHWOOD, 1987). LOCKWOOD and FULLER-ROWELL (1987a,b) have predicted that non-thermal plasma will also occur following sudden changes in the convection pattern, such as during substorms and following increases in the cross-cap potential, as reported recently by LOCKWOOD et al. (1986a,b). The plasma was predicted to be furthest from thermal equilibrium in the convection 'throat' and in the dawnside auroral oval. FARMER et al. (1988) have presented spectra characteristic of non-thermal plasma, also observed using U.K.–POLAR, which persisted for over an hour in the dawn auroral oval following the major expansion of the polar cap described by LOCKWOOD et al. (1986b). In addition, MOORCROFT and SCHLEGEL (1988) have shown that the statistical occurrence of exceptionally high T_{im}, deduced from EISCAT Common Programme CP-3-C data with the assumption of a Maxwellian ion velocity distribution, is similar to that predicted for the longitude of EISCAT by FARMER et al. (1988) from the modelling of LOCKWOOD and FULLER-ROWELL (1987a,b). WINSER et al. (1987) have shown that the aspect angle dependence of the shape and width of spectra from the EISCAT CP-3-E experiment is as predicted by RAMAN et al. (1981) during periods of large ion drifts.

The simulations of the effects of non-Maxwellian plasma on the spectrum of incoherent scatter signals by RAMAN et al. (1981) and HUBERT (1984) employed ion velocity distribution functions based on the retarding potential analyser data from AE-C (ST.-MAURICE et al., 1976). They also assumed that the plasma remained homogeneous within the scattering volume. OTT and FARLEY (1975) and ST.-MAURICE (1978) have discussed various instabilities which may be driven by non-Maxwellian, anisotropic or toroidal ion velocity distributions. These authors concluded that the Post–Rosenbluth instability (ROSENBLUTH and POST, 1965) has the lowest threshold for the form of distribution function inferred by ST.-MAURICE et al. (1976). The Post–Rosenbluth is an electrostatic micro-instability which, at least according to linear theory, propagates with a wave vector almost perpendicular to the magnetic field. ST.-MAURICE (1978) has used linear theory to demonstrate how the drift threshold for this instability is dependent on ion composition and showed that, for the simple relaxation model of the ion–neutral collision process, this threshold is 1.3–2.0 times the thermal speed of the neutral gas. There are two ways in which an instability could affect the scattered spectrum for signals incident at angles approaching 90° to the geomagnetic field: the first is through its effect on the line-of-sight ion velocity distribution function by diffusion of resonant ions in velocity space and the second is the addition of coherent-like echoes from the density fluctuations associated with the instability. Recently, SUVANTO (1987) has discussed the effects of the Post–Rosenbluth instability on the ion velocity distribution function, but the density irregularity spectrum remains unknown.

In this paper we investigate the effect of non-thermal plasma on the scattered signal during several of the short-lived flow burst events described by TODD *et al.* (1986, 1988), assessing the possible role of density irregularities in the lower *F*-region when the ion drift exceeds the Post–Rosenbluth instability threshold.

2. OBSERVATIONS

All the data presented here have been recorded on two days by EISCAT using the U.K. Special Programme U.K.–POLAR (VAN EYKEN *et al.*, 1984; WILLIS *et al.*, 1986). This experiment uses the UHF radar with a beam elevation of 21.5°. Data of sufficiently high signal-to-background ratio for 15 s resolution are here obtained from the first 6 or 7 of 12 continuous range gates. These gates are centred on ranges $r = 450+75n$ km, heights $h \approx 175+34n$ km and invariant latitudes $\Lambda \approx 70.2+0.6n°$, where n is the gate number. The data for 27 October 1984 are from a beam-swinging version of the experiment, but are not used here to derive convection vectors: instead, they are regarded as 15 s l-o-s scalar data taken along two separate azimuths, as in the paper by TODD *et al.* (1988). The data for 25 August 1985 are for a single look direction at azimuth 344° (along the *L*-shell meridian). In this paper we concentrate on three 10 min periods; 06 : 35–06 : 45 UT on 27 October 1984 and 08 : 03–08 : 13 UT and 08 : 13–08 : 23 UT on 25 August 1985. These periods are selected because they contain poleward flow bursts, of the kind presented by TODD *et al.* (1986), and spectra indicating non-thermal plasma, as discussed by LOCKWOOD *et al.* (1987).

2.1. *Data for 27 October 1984*

The l-o-s velocities v_T observed in range gates 1–6 during the period 06 : 26–06 : 50 UT have been presented in fig. 1 of TODD *et al.* (1986). This period contains two poleward flow burst events, the first commencing shortly before 06 : 35 UT and the second following roughly 5 min later. In Fig. 1(d) we plot 15 s pre-integrated values of v_T for gate 3 only (mean altitude 277 km), with solid circles indicating poleward flow and open circles denoting equatorward flow, explained by TODD *et al.* (1986) as the central, poleward and return flows of the twin-vortex flow

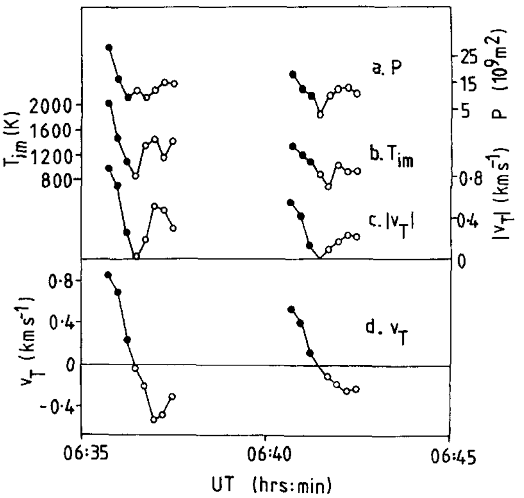

Fig. 1. U.K.–POLAR observations for gate 3 on 27 October 1984: (a) the range-corrected signal to background power ratio P (= the scattered power S divided by the background noise power N and multiplied by the square of r, the range); (b) the ion temperature deduced assuming a Maxwellian ion velocity distribution T_{im}; (c) the modulus of the line-of-sight velocity $|v_T|$; (d) v_T. Solid circles are for flows away from and open circles for flows towards the radar (roughly poleward and equatorward, respectively).

pattern, respectively. Only the data from azimuth 356 (12° east of magnetic north) are used, because, as we shall see, the axis and poleward flows of the twin vortex are reasonably well aligned with this azimuth. Figures (a), (b) and (c) compare the observed temporal variations of P, T_{im} and $|v_T|$, respectively, where P is r^2. S/N (where S is the signal power, N is the background noise power and r is the range of the scattering volume from the radar) and T_{im} is the ion temperature deduced using a Maxwellian ion velocity distribution. Figure 1 reveals strong correlations between these three variables.

Figure 2 shows the spectra for the first four data points presented in Fig. 1. The first three of these 15 s spectra reveal the form predicted by RAMAN *et al.* (1981) for non-Maxwellian ion velocity distributions, driven by large drifts in the presence of ion–neutral collisions. Experimental spectra of this form have also been reported by LOCKWOOD *et al.* (1987) and WINSER *et al.* (1987). As the observed l-o-s velocity drops to zero at the boundary between the poleward and equatorward flow, which is encountered near 06 : 36 : 15 (Fig. 1), the spectra return to the normal twin-peaked form expected for a Maxwellian plasma. Figure 1 shows that both the scattered power and the ion temperature estimate T_{im} show clear minima at this boundary (where v_T is zero) for both the flow bursts in this period. The spectrum shown in Fig. 2(c)

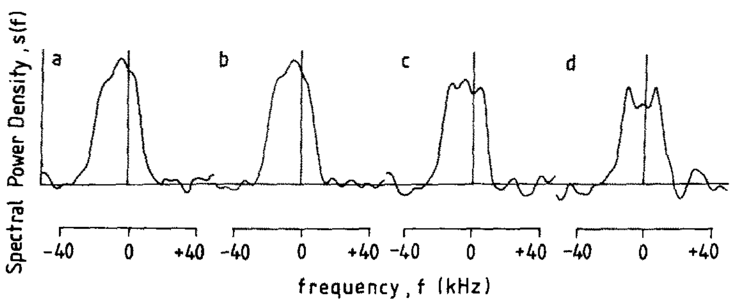

Fig. 2. Observed spectra for gate 3 on 27 October 1984 for 15 s pre-integration periods ending at: (a) 06:35:30 UT; (b) 06:35:45 UT; (c) 06:36:00 UT; (d) 06:36:15 UT.

is the same as for gate 3 in fig. 1 of LOCKWOOD *et al.* (1987), which gives the spectra in gates 2–5 at 06:36:00 UT and is repeated here in Fig. 3(a). Comparison of Figs. 2 and 3(a) shows that both the temporal and spatial variations reveal spectra characteristic of non-Maxwellian plasma when v_T is large ($> 0.75\,\mathrm{km\,s^{-1}}$), but not when and where v_T is smaller.

Figure 3 also demonstrates how the characteristic spectral form of these data can be explained by non-Maxwellian ion velocity distribution functions. Figure 3(c) shows synthesised spectra, using the RAMAN *et* al. (1981) procedure, for the U.K.–POLAR look direction (which makes an angle $\Phi = 73.5^\circ$ with the geomagnetic field) assuming an ionic composition of 100% O^+ and an electron temperature T_e of 3500K, which is the optimum for fitting the observed spectra. These spectra were synthesised using distribution function deformation factors D^* (as defined by RAMAN *et al.*, 1981) of 0.4, 0.9 and 1.4. It can be seen that as D^* increases a central peak to the spectrum emerges (at the frequency corresponding to the mean Doppler shift) and the ion-acoustic peaks are reduced to shoulders, decrease in size and move away from the centre of the spectrum. The one-dimensional l-o-s ion velocity distribution functions corresponding to these spectra (for the same D^*) are shown in Fig. 3(b). For $D^* = 0.4$ the distribution function is very close to a Maxwellian. As D^* is increased the distribution function is flattened at low ion speeds, until for $D^* = 1.4$ the distribution becomes flat topped. Any further increase in D^* would cause the distribution of field-perpendicular velocities to form a minimum at the origin, i.e. the distribution function becomes toroidal. The reduction of the distribution function near zero velocity causes the central peak of the spectrum to emerge by reducing the dielectric function, which appears in the denominator of expressions for the spectral power density. The slope of the distribution function at the ion-acoustic frequency is increased by the increase in D^* and this causes increased Landau damping of the normal ion-acoustic peaks of the spectrum. In addition, in the vicinity of both the up- and down-shifted ion-acoustic frequencies the slope, and hence Landau damping, decreases with increasing frequency magnitude, which has the effect of moving the ion-acoustic peaks apart as they evolve into inflexion points as D^* increases.

The correlation between T_{im}, P and $|v_T|$ noted above (and shown in Fig. 1 for gate 3) are confirmed by fig. 2 of LOCKWOOD *et al.* (1987) for all gates and by Fig. 4 of this paper, which is for gate 4 only. Figure 4 shows scatter plots and regression lines for P and T_{im} as functions of v_T^2 [Figs. 4(a) and (b), respectively], as well as one for P as a function of T_{im} [Fig. 4(c)]. As both P and T_{im} vary approximately as the square of v_T, P should vary approximately linearly with T_{im}. The significance of these correlations will be discussed in the following section, in the light of the corresponding data for 25 August 1985. LOCKWOOD *et al.* (1987) have shown that the slope of these regression lines is too great to allow any explanation in terms of a bi-Maxwellian ion velocity distribution and hence, along with the characteristic spectra, these regressions show that the plasma is non-Maxwellian.

2.2. *Data for 25 August 1985*

The line-of-sight velocities v_T observed on 25 August 1985 are shown in Fig. 5 Exceptionally large peaks of l–o-s velocity are observed in two periods around 08:05 and 08:15 UT and these are particularly clear at the lower latitudes (gates 1–3). In addition, there is a burst around 08:08 UT which can be seen in gates 3 and 4 (and to a very small extent in gate 2). Gate 4 shows a more gradual enhancement around the 08:08 event. In order to obtain sufficient samples in a data subset we divided these data into just two periods: from 08:03 UT (the start of the dataset) to 08:13 UT and from 08:13 to 08:23 UT.

In order to study the scattered power and ion temperatures for these data Fig. 6 shows P and T_{im}

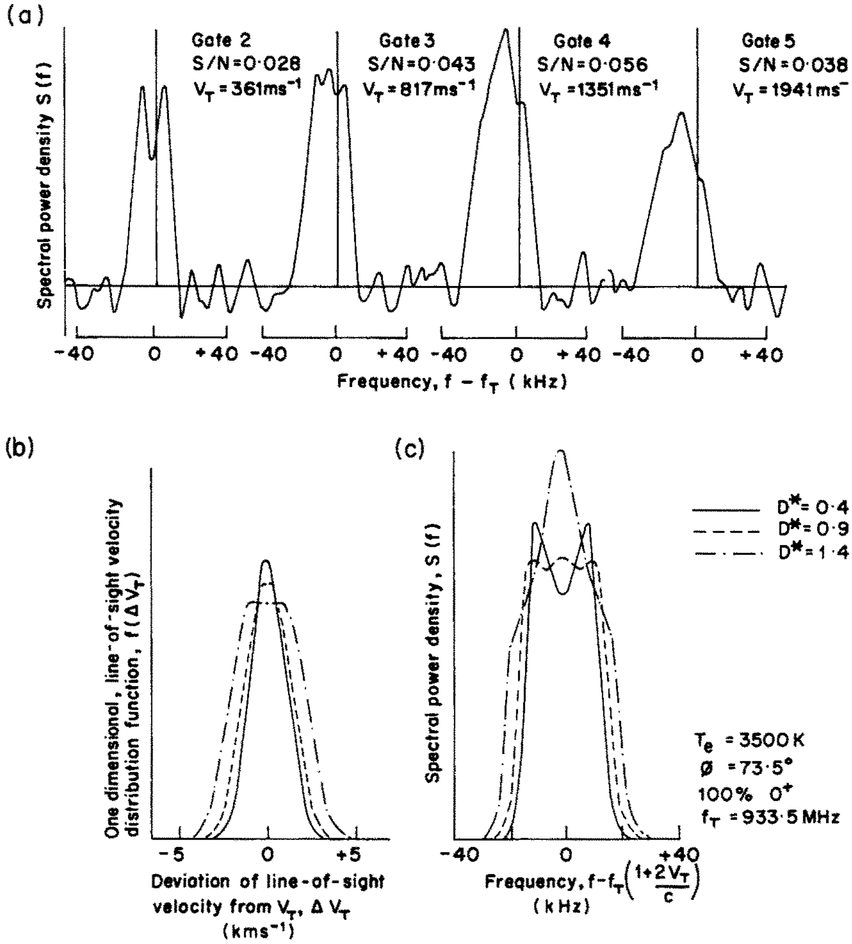

Fig. 3. (a) Observed spectra for gates 2–5 for the pre-integration period ending 06 : 36 : 00 UT on 27 October 1984. (b) Synthesised line-of-sight (at angle, $\Phi = 73.5°$ to the geomagnetic field) ion velocity distributions $f(\Delta v_T)$ as a function of Δv_T, the deviation of the line-of-sight from the average (bulk flow) velocity v_T, shown for D^* values of 0.4, 0.9 and 1.4. (c) Synthesised spectra for the distribution functions shown in (b) for $T_e = 3500$K, ionic composition of 100% O^+ and the EISCAT UHF radar frequency f_T of 933 MHz. Note that in (c) the Doppler shift due to the bulk flow v_T has been removed so all spectra are centred on the origin of the plot.

plotted as a function of UT for gate 3. Comparison of Fig. 6 with the panel of Fig. 5 for gate 3 shows that the behaviour of the three parameters P, T_{im} and v_T is much less clear than for the 27 October event. The scattered power, and hence P, reveals large and rapid fluctuations, sometimes accompanied by similar variations in T_{im}, but not v_T (as near 08 : 07 : 30 UT), but at other times without any changes in T_{im} (as around 08 : 10 and 08 : 13 UT). Note that, as well as containing some exceptionally high velocities, these data show remarkably high T_{im} values throughout, but especially around 08 : 07 : 30, where T_{im} reaches 7500K. The 15 s spectra at these times have clear central peaks with only shoulders at the ion-acoustic frequency, indicating that the ion velocity distribution is non-Maxwellian and hence T_{im} is likely to be an over-estimate of the real l-o-s temperature T_f (RAMAN *et al.*, 1981). Moreover, as the angle between the look direction and the geomagnetic field is $\Phi = 73.5°$ for these observations, any anisotropy will cause T_f to exceed the average ion temperature T_i. The values of P are also remarkably high during this period: the peak values correspond to a signal-to-background ratio (S/N) of over 15%. This compares with 5% at the beginning and end of the period, which is typical for this U.K.–POLAR gate, near the $F2$-peak. From

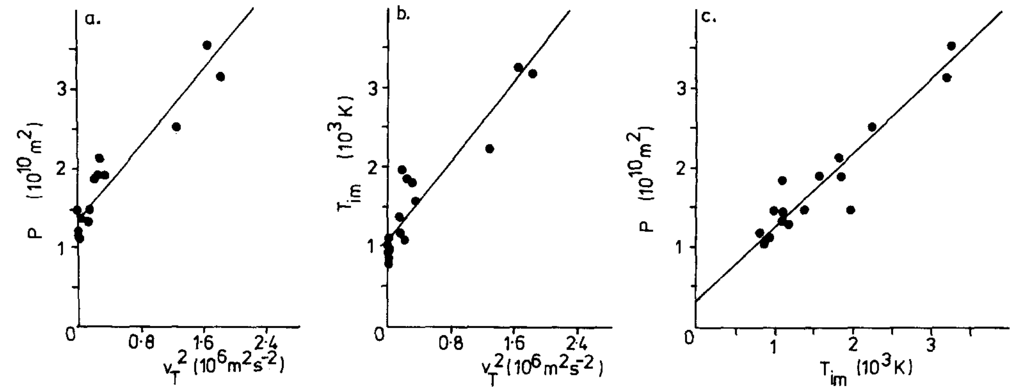

Fig. 4. Scatter plots and linear regression fits for: (a) P against v_T^2; (b) T_{im} against v_T^2; (c) P against T_{im}. All data are 15 s pre-integrations for gate 4, azimuth 356° and the period 06:35–06:45 UT on 27 October 1984.

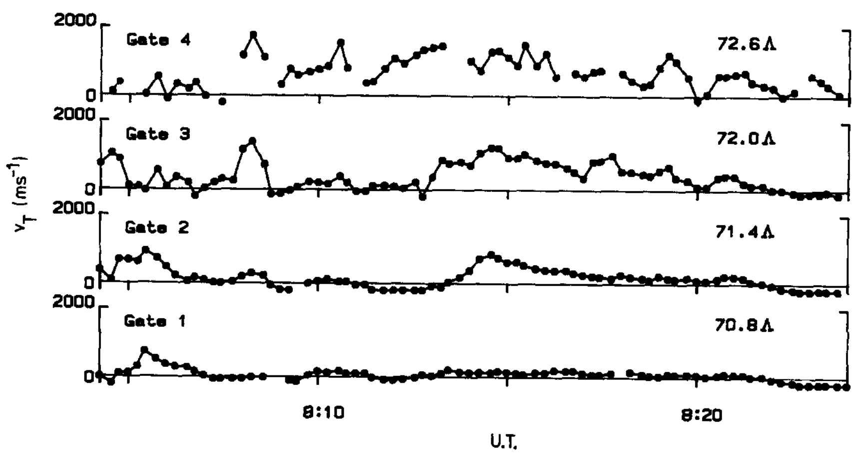

Fig. 5. Line of sight velocities v_T observed in gates 1–4 for azimuth 344° on 25 August 1985.

these values of S/N we compute the error in S to be roughly 5% before and after the peak of received power, falling to below 2% at the peak.

Figure 7 shows examples of observed spectra for gate 3, post-integrated into the 1 min periods labelled (a–h) in Fig. 6. It can be seen that for the first 3 min (a–c), when P is relatively more enhanced than T_{im}, the spectra are single humped and asymmetric with an enhancement to the downward Doppler-shifted side of the spectrum (corresponding to motion away from the radar, i.e. poleward). This persistent asymmetry is more clearly seen in the 15 s spectra in Fig. 8 (for which the signal-to-background ratio is smaller) and is most pronounced at the peaks in P shown in Fig. 6. The arrows in Fig. 6(a) mark the data points corresponding to the spectra shown in Fig. 8. The asymmetry appears and disappears very rapidly (on time scales of about 30 s), in phase with rises and falls in the scattered power (Fig. 6). This is demonstrated by Figs. 8(a) and (b). The spectrum in Fig. 8(a) is typical of that predicted for non-thermal plasma by RAMAN *et al.* (1981), with a central peak and only shoulders at the up- and down-shifted ion-acoustic frequency (indicating relatively low T_eT_i). The value of P for this pre-integrated dump (08:11:45–08:12:00 UT) is $5.0 \cdot 10^{10}\,m^2$ and the fitted temperature T_{im} is 4047K. Thirty seconds later, for 08:12:15–08:12:30 UT, the spectrum is asymmetric, as the peak near the down-shifted ion-acoustic frequency has grown and the total power has risen, giving P of $8.1 \cdot 10^{10}\,m^2$, without much rise in spectrum width as T_{im} has only risen to 4200K. The peak near the down-shifted ion-acoustic frequency is always observed when P is a maximum, but is most marked for narrower spectra, for example 08:17:00–08:17:15 UT [Fig. 8(d)], for which T_{im} is 3006K.

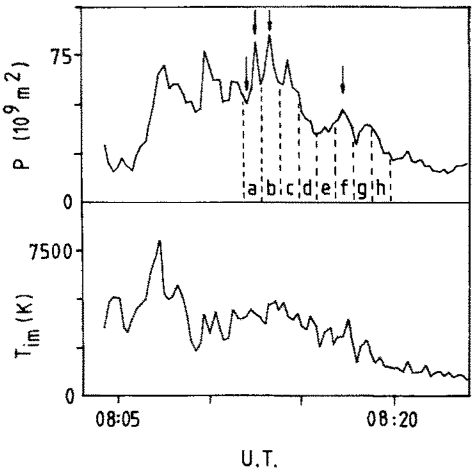

Fig. 6. (a) Range-corrected signal to background noise ratio P and (b) ion temperature estimate T_{im} shown as a function of UT for gate 3 on 25 August 1985. Periods marked (a–h) yield the post-integrated spectra shown in Fig. 7. The arrows mark the data points corresponding to the 15 s spectra shown in Fig. 8.

As the power and the fitted ion temperature T_{im} continue to drop [periods (d) and (e) in Fig. 7] two-humped spectra begin to appear, but the asymmetry returns during a rise of power in period (f). Periods (g) and (h) and all subsequent periods show double-peaked spectra, typical of Maxwellian F-region plasma.

The scatter plots shown in Fig. 9 are similar to those presented in Fig. 4, but are for gate 3 during the period 08:13-08:23 UT on 25 August 1985. In this case no clear correlations of T_{im} nor of P with v_T^2 are apparent. However, it is true that for both scatter plots all points lie above a divider, shown as a dashed line, with no points to the low T_{im}-high v_T^2 side of this line. For ion drift velocity v_i which greatly exceeds the neutral wind speed an isotropic Maxwellian would have a temperature $T_{im} = T_i$, which is proportional to v_i^2 by the frictional heating equation (ST.-MAURICE and HANSON, 1982): note that v_T is the component of v_i along the radar line of sight. In addition, a rise in scattered power is expected with increasing v_i, due to the rise in T_i (see the following section). It is therefore

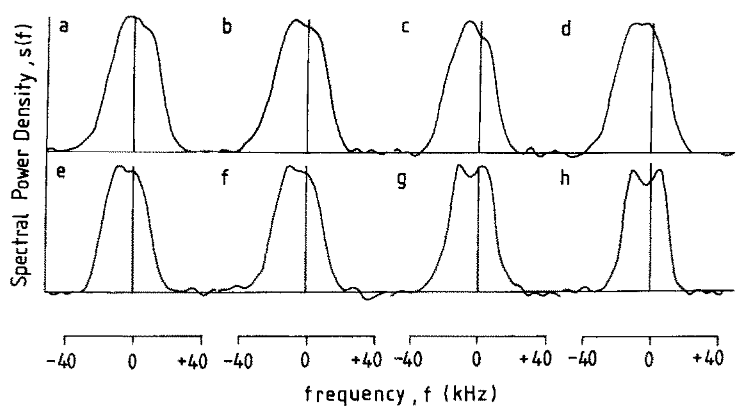

Fig. 7. One minute post-integrated spectra for gate 3 for the periods commencing (a) 08:11:45, (b) 08:12:45, (c) 08:13:45, (d) 08.14:45, (e) 08:15:45, (f) 08:16:45, (g) 08:17:45 UT and (h) 08:18:45 UT on 25 August 1985. Periods (a–h) are marked in Fig. 5.

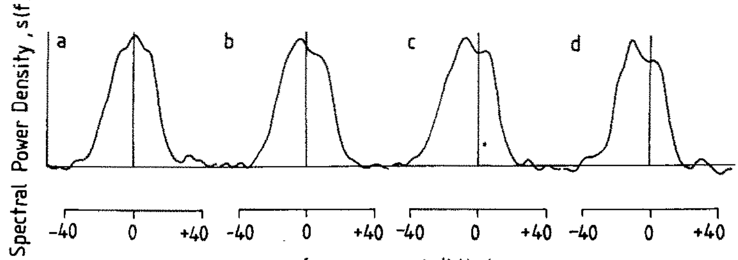

Fig. 8. Observed spectra for gate 3 on 25 August 1985 for 15s pre-integrated periods ending at: (a) 08:12:15 UT; (b) 08:12:30 UT; (c) 08:13:15 UT; (d) 08:17:15 UT. The range-corrected signal to background noise ratio for these spectra are given by the data points marked with arrows in Fig. 5.

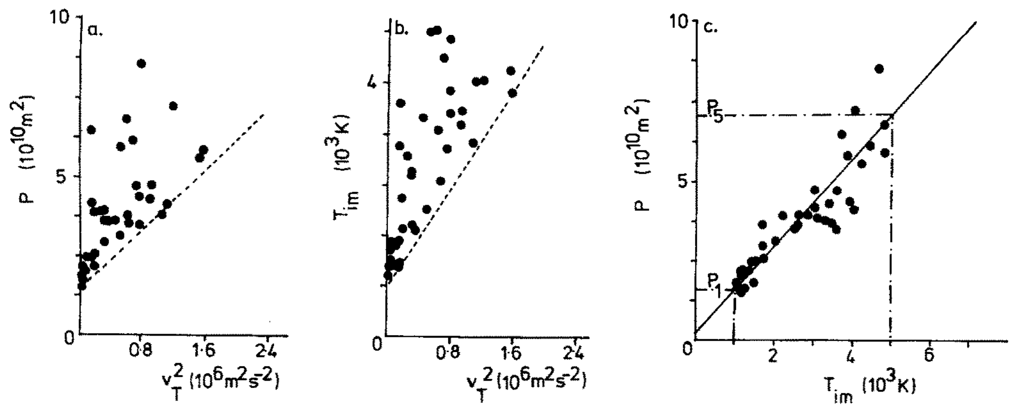

Fig. 9. As Fig. 3, but for gate 3 during the period 08 : 13–08 : 23 UT on 25 August 1985 (azimuth = 344°).

possible to explain the deviations from a linear form in Figs. 9(a) and (b) by a large angle between v_i and the radar line-of-sight, so there is a large cross-beam flow and $v_T < v_i$. Conversely, the approximate linearity shown in Figs. 4(a) and (b) implies that $v_T \approx v_i$, i.e. that the flow is largely aligned along the line-of-sight for the 27 October event. We conclude that for 25 August there are significant east–west flows. However, these should not effect the linearity between the two scalar quantities T_{im} and P, and Fig. 9(c) indicates that this is indeed the case.

The approximately linear dependence of P on the apparent ion temperature T_{im} is observed in nearly all gates for all the periods discussed in this paper, although gates 4 and 5 tend to show considerably more spread than either higher or lower number gates. This is demonstrated by Fig. 10, which shows the scatter plots for gates 1–6 during the same period. There is a clear tendency for the slope of the regression fit to decrease with increasing gate number. It should be remembered that these U.K.–POLAR observations are made with a radar beam elevation of 21.5° and that invariant latitude as well as altitude increases with gate number.

It is useful to define a power gain h from experimental scatter plots of the kind shown in Figs. 4(c) and 9(c)

$$h = 10 \cdot \log_{10}(P_5/P_1), \tag{3}$$

where P_1 and P_5 are the values of P when the deduced ion temperature T_{im} is 1000K and 5000K, respectively. Figure 9(c) demonstrates how P_5 and P_1, and hence h, can be quantified from regression fits of the kind also shown in Figs. 4(c) and 10. Uncertainties in h are estimated using the maximum and minimum slopes of the regression line for plus and minus 2 standard deviations from the mean slope. These errors are therefore related to the correlation coefficients, which are always large and close to unity, particularly for the nearer range gates.

3. SCATTERED POWER FROM MAXWELLIAN AND NON-MAXWELLIAN, HOMOGENEOUS PLASMAS

The well-known equation for the total scattered power (sum of the electron and ion line spectra) from an isotropic, homogeneous, Maxwellian plasma is (BUNEMAN, 1962; MOORCROFT, 1963; BEYNON and WILLIAMS, 1978)

$$S = (G\sigma_e N_e/r^2)[1-(1+\alpha^2)^{-1} + \{(1+\alpha^2)(1+\alpha^2+T_e/T_i)\}^{-1}], \tag{4}$$

where G is the radar gain (which includes the effective aperture of the antenna, the radiated power and the pulse length), r is the range, N_e the plasma density, σ_e is the electron scattering cross-section and

$$\alpha = 4\pi\cos(\Theta/2)D/\lambda \approx (4\pi/\lambda)\cdot\cos(\Theta/2)\cdot 69(T_e/N_e)^{0.5}, \tag{5}$$

where λ is the radar wavelength, D is the Debye length and Θ the angle between the transmitter and receiver beams. For the backscatter considered here $\Theta = 0$. The first two terms in the brackets of equation (4) are for the electron line, the third is for the ion line spectrum. The bandwidth of U.K.–POLAR (100 kHz) results in the reception of power only in the ion line (EVANS, 1969). In order to directly compare the power returned by different range gates, it is useful to define a variable P as the signal-to-background ratio multiplied by the square of the range. For a Maxwellian plasma P is therefore given by

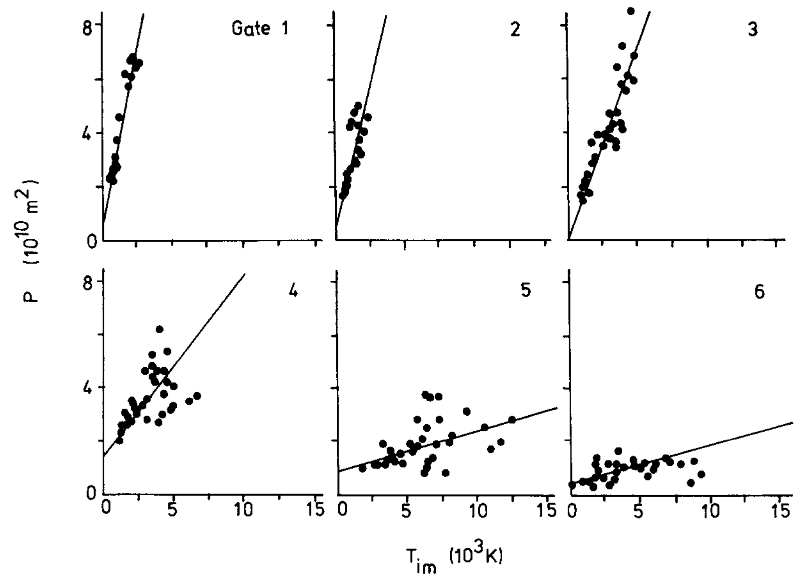

Fig. 10. Scatter plots and linear regression fits of P as a function of T_{im} [as in Figs. 3(c) and 8(c)] for gates 1–6 and the period 08 : 13–08 : 23 UT on 25 August 1985.

$$P = (S/N)\cdot r^2$$
$$= k\cdot N_e[(1+\alpha^2)(1+\alpha^2+T_e/T_i)]^{-1}, \quad (6)$$

where k $(= G\sigma_e/N)$ is a constant for constant background noise power N. Note that equations (4)–(6) are only valid for small T_e/T_i, MOORCROFT (1963) having shown that the effective cross section becomes σ_e if $T_e/T_i > 10$.

From the definition of gain h due to a rise in ion temperature T_i from 1000K to 5000K [equation (3)], we have for a thermal plasma

$$h = 10\log_{10}\left[\frac{(1+\alpha^2+T_e/1000)}{(1+\alpha^2+T_e/5000)}\right]. \quad (7)$$

This equation assumes that there is no change in the plasma density, electron temperature, ion composition or α during the rise in ion temperature. The implications of these assumptions on the validity of applying equation (7) to the data presented in this paper are addressed in the discussion.

At present there is no analytic expression, corresponding to equation (4), for the power scattered by a homogeneous non-Maxwellian plasma. The power can be computed numerically using the method of RAMAN *et al.* (1981). Results for the U.K.–POLAR look direction are shown in Fig. 11. The power computed by the Raman *et al.* procedure S_R is plotted as a function of the ion velocity distribution deformation parameter D^* (for an isotropic Maxwellian $D^* = 0$) : D^* values are shown along the horizontal axis at the top of Fig. 11. The simulations of the scattering process were carried out for three electron temperatures T_e of 2500, 3000 and 3500K. For each simulation it is possible to use equation (4) to evaluate the power scattered by an isotropic Maxwellian plasma S_i for the same α, T_e and T_i, where T_i is the three-dimensional ion temperature of the non-thermal plasma (as defined by RAMAN *et al.*, 1981; MOORCROFT and SCHLEGEL, 1988). Figure 11 indicates that S_R is very similar to S_i—the upper panel plots S_R/S_i and shows that they are the same to within 6% at $T_e = 2500$K, falling to within 2% at $T_e = 3500$K. We know of no analytic derivation of this numerical result, nor have we attempted to show that it is valid over a wide range of α, T_e and T_i by a parametric survey of numerical results. However, similar numerical calculations have led other scientists to the same conclusion (BUCHERT, 1987; MOORCROFT, 1987).

The D^* axis in Fig. 11 has been calibrated in terms of the ion drift v_i and non-dimensional ion drift D' $(= v_i/v_{th}$, where v_{th} is the two-dimensional thermal speed of the neutral gas). The study of retarding potential analyser (RPA) data from the AE-C satellite by ST.-MAURICE *et al.* (1976) yielded an empirical relationship between D^* and T_i. In addition, D' (and hence v_i) is related to T_i, for a given T_n, by the frictional heating equation (ST.-MAURICE and HANSON, 1982). The axes shown at the bottom of Fig. 11 have employed the ST.-MAURICE *et al.* (1976) relationship with a T_n of 1000K—a value inferred for both the 25

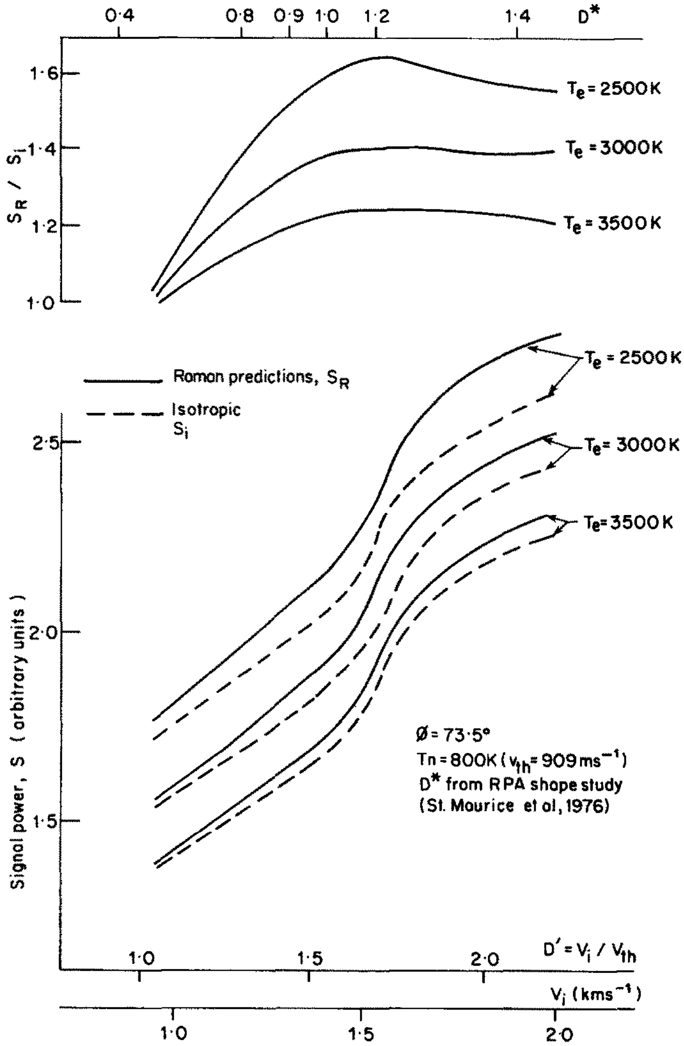

Fig. 11. Scattered power for non-Maxwellian plasma S_R computed numerically by the RAMAN *et al.* (1981) procedure and evaluated for a Maxwellian plasma using equation (4), S_i shown as a function of ion drift v_i, D' and D^* (see text) for a neutral temperature T_n = 1000K and electron temperature T_e of 2500K, 3000K and 3500K. The upper panel shows the ratio S_R/S_i.

August and 27 October events discussed here (see LOCKWOOD *et al.*, 1987, and the intercepts of the regression lines of Figs. 4a and 9a). It is interesting to note that the power rise shown by the regression in Fig. 4(a) for an increase in velocity ($v_T \approx vi$ for this event) from 1.0 to 1.5 km s^{-1} is 1.5+0.2 dB: the corresponding power gains from Fig. 11 are 1.0, 1.05 and 1.1 dB for T_e of 2500, 3000 and 3500K, respectively. Hence the observed power rise is considerably larger than that simulated for the non-Maxwellian plasma. However, it is not possible to tell if this difference is significant, as v_i may have exceeded v_T by an unknown factor.

Both RAMAN *et al.* (1981) and HUBERT (1984) have pointed out that if the plasma is non-thermal, the temperatures deduced from fitting a spectrum derived from a Maxwellian ion velocity distribution T_{im} and T_{em} differ from the true l-o-s values T_f and T_e. In addition, the one-dimensional l-o-s ion temperature T_f will not equal the average three-dimensional ion temperature T_i if the plasma is anisotropic. For the range of ion drifts considered by these authors (giving D^* values up to 3.0) and for an O^+ dominated plasma they found that $T_{im} > T_f > T_i$ (for Φ greater than 54.7° as here) and $T_{em} < T_e$, hence for such cases the ratio (T_{em}/T_{im}) is smaller than its true value (T_e/T_i). If larger drifts are considered, these inequalities can be reversed (HUBERT, 1987; BUCHERT 1987): this occurs at a lower drift for NO^+ than for O^+. MOORCROFT and SCHLEGEL (1988) have reported that deviations from thermal plasma ($D^* > 0$) are accompanied by rises in T_{im} and decreases in T_{em} at 325 km altitude. We conclude that at these altitudes (where the plasma is normally dominated by O^+) the drifts are not usually large enough to reverse the inequalities. We define a factor F to be

$$F = (T_{em}/T_{im})/(T_e/T_i) \tag{8}$$

and, if the drifts are not large enough to reverse the above inequalities, we have $0 < F < 1$. We expect that this is normally the case, but note that it is possible for F to exceed 1 if the plasma is very highly non-thermal, particularly if it is dominated by NO^+.

Using equation (8) and the result that the power scattered by a non-Maxwellian plasma is (at least approximately) the same as that scattered by an isotropic Maxwellian plasma of the same T_e and T_i, we can generalise equation (6) to predict the power scattered by a non-thermal plasma in terms of the temperatures derived by assuming a Maxwellian ion velocity distribution, T_{em} and T_{im},

$$P = k \cdot N_e\{(1+\alpha^2)[1+\alpha^2+T_{em}/(F \cdot T_{im})]\}^{-1} \tag{9}$$

and hence equation (7) for the observed gain h can be generalised, for cases where α and T_{em} remain constant, to

$$h = 10\log_{10}\left\{\frac{[1+\alpha^2+T_{em}/(F_1 \cdot 1000)]}{[1+\alpha^2+T_{em}/(F_5 \cdot 5000)]}\right\}, \tag{10}$$

where F_1 and F_5 are the values of F when T_{im} is 1000K and 5000K, respectively.

4. OBSERVED RELATIONSHIP BETWEEN SCATTERED POWER AND INFERRED ION TEMPERATURE T_{im}

In order to use equations (9) and (10) to predict the variation of scattered power with the inferred ion temperature T_{im} we must determine α and T_{em}. For all the gates, and all three periods, we find that the fitted values of both α and T_{em} tend to decrease a small amount with increasing T_{im}. This is demonstrated by Fig. 12 for gate 3 during the interval 08:13–08:23 UT on 25 August 1985. Note that the slight decrease of T_{em} with T_{im} is consistent with the findings of MOORCROFT and SCHLEGEL (1988) and indicates non-thermal plasma with $F < 1$. Using the average values for α and T_{em} (0.43 and 2112K, respectively), the curves shown in Fig. 13 are plotted using equation (9) and a variety of values for F. Superposed on these curves are the data points for this period and it is immediately apparent that the curves, and hence equation (10), are incapable of explaining the observations giving large T_{im} and P, even if F exceeds 1. The data for lower T_{im} (< 2500K) and P do agree reasonably well with the curve for $F = 1$ (Maxwellian plasma): note that N_e has been chosen to give a good fit to these data points. A variety of possible reasons for this behaviour will be discussed in the following section.

It is useful to compare Fig. 13 with the corresponding plot for a higher altitude. Figure 14 shows data for gate 6 during the interval 08:03–08:13 UT on the same day. The curves have been plotted using the average values of α and T_{em} for this period, namely 0.463 and 3140K, respectively. In this example the data indicate lower F values at larger T_{im}, i.e. the data are explained by equation (10) and are consistent with non-thermal plasma, causing T_{im} to be an overestimate of T_i. This is also expected from the very high values of T_{im} observed (up to 9000K).

Figure 13 is typical of the behaviour observed for all gates at altitudes below about 300 km (gates 1–3). Figure 14 is typical of observations at greater altitudes (gates 4–6). This is demonstrated by Fig. 15, which shows the gain h observed for gates 1–6 in all 3 intervals discussed in this paper. The solid points show the observed values from the regression fits to the data, calculated from equation (3) using P_5 and P_1 values scaled as shown in Fig. 9(c). The open circles are calculated using equation (10) with average α and T_{em} values for the entire 10 min interval and taking $F_5 = F_1 = 1$ (isotropic Maxwellian plasma). Errors in the computed h values are evaluated from the standard deviations of α and T_{em}. It can be seen that for all three periods we have increases in signal strength which are too great (by up to 5 dB) to be explained by equation (10), even allowing for the expected errors in both the observed and predicted h. These anomalous increases are only observed at lower altitudes (gates 1 to about 3). Generally, the power gain h falls gradually with gate number to values lower than predicted by equation (10) for the further range gates (5 and 6). For some of the further gates the difference sometimes exceeds the sum of the errors in the h values and these significant differences can be explained by equation (10) if $F < 1$, i.e. the plasma is non-Maxwellian but homogeneous.

5. DISCUSSION

Although T_{im} is not, in general, equal to the real ion temperature T_i a rise in T_{im} does indicate a rise in T_i for the $\Phi = 73.5°$ of these observations. This is true

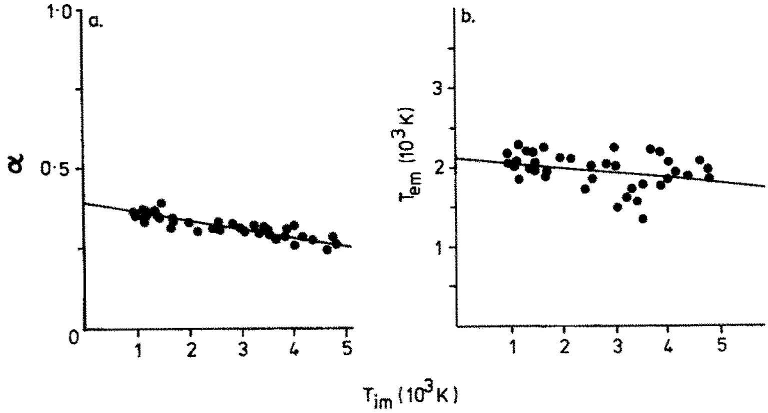

Fig. 12. Scatter plots of fitted values of (a) α and (b) electron temperature T_{em} as a function of observed ion temperature T_{im} for gate 3 and the period 08 : 13–08 : 23 UT on 25 August 1985.

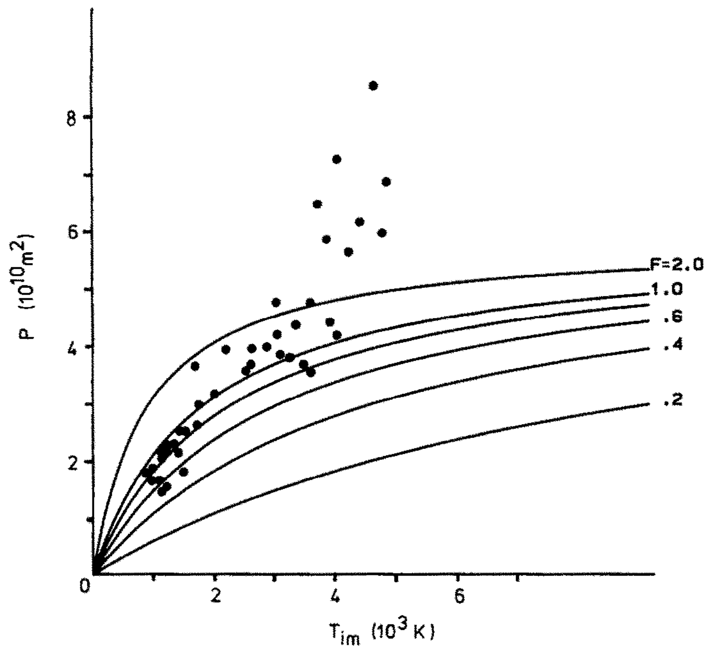

Fig. 13. Curves of P as a function of T_{im} plotted for various F factors (see text) using equation (8) and average values for T_{em} and α of 2112K and 0.43, respectively (Fig. 12). Superposed are data from gate 3 during the period 08 : 13–08 : 23 UT on 25 August 1985.

provided that there is not a large spread of l-o-s bulk velocities, either within the scattering volume or during an integration period, which can raise T_{im} (but not T_i) by smearing the spectrum. However, the ratio of the ion line width to the mean Doppler shift is sufficiently large to make the increases in T_{im} due to this smearing effect typically much smaller than that reported here. Much larger increases in T_{im} are expected, due to anisotropic ion velocity distributions, if $\Phi > 54.7°$ (RAMAN et al., 1981), and also due to the distortion of the l-o-s ion velocity distribution function from a Maxwellian form. Both these effects are expected in the presence of large ion drifts (relative to the neutral gas), which also raise T_i by frictional heating. Hence, for these U.K.–POLAR data we expect an observed rise in T_{im} to indicate a rise in the real ion temperature T_i.

It has been demonstrated in the previous section that the increase in scattered power accompanying an observed rise in apparent ion temperature T_{im} is

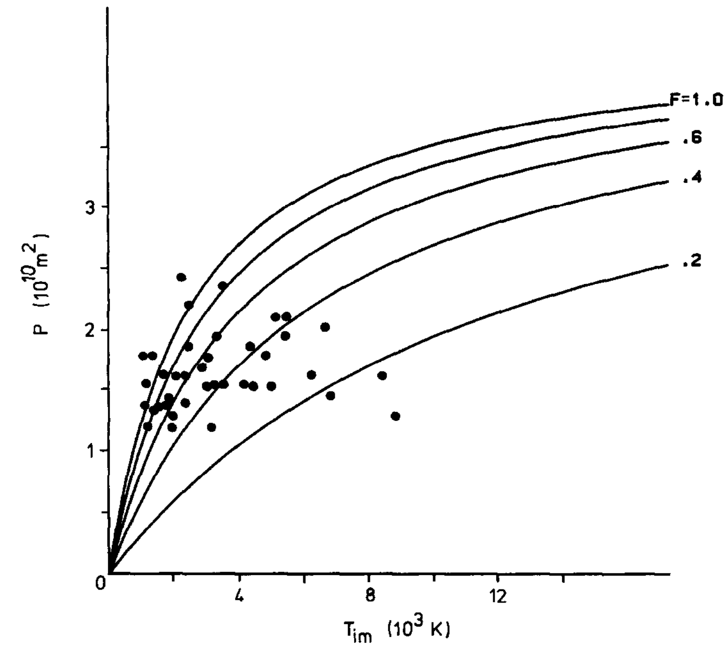

Fig. 14. As Fig. 13, but for gate 6 during the period 08 : 03–08 : 13 UT on 25 August 1985, for which average T_{em} and α are 3140K and 0.463, respectively.

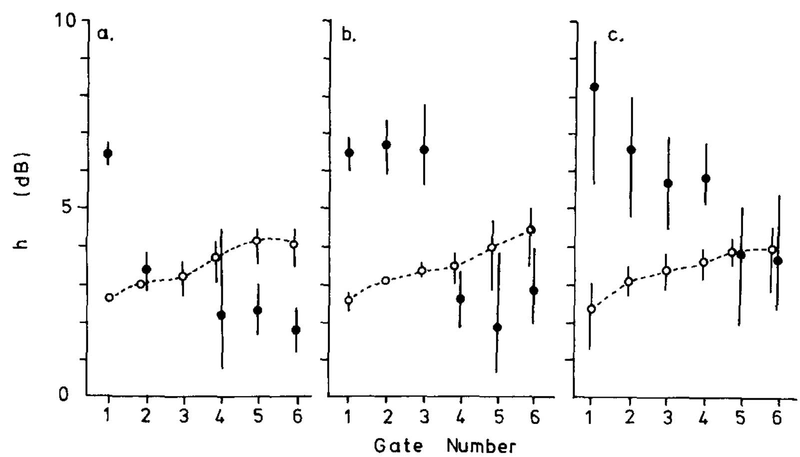

Fig. 15. Observed values of the gain h for gates 1–6 (solid circles) from regression fits of P against T_{im} and values computed from equation (10) (open circles) for $F_1 = F_5 = 1$ and average values for T_{em} and α: (a) for 08:03–08:13 UT on 25 August 1985; (b) for 08:13–08:23 UT on 25 August 1985. (c) for 06:35–06:45 UT on 27 October 1984.

anomalously large [compared to that predicted by equation (10)] for the lower altitude gates. From the above argument we deduce that the power rise must also be accompanied by an increase in the real ion temperature T_i. Bearing this in mind, the following discussion explores a number of possible explanations for the power rise and the asymmetric spectral shape at times of high power. In order to do this, we will first consider explanations in terms of 'incoherent scatter', by which we mean scatter which is due to thermal fluctuations in the plasma. Then, in Section 5.2, we will consider the addition of power scattered by some other mechanism, which we will term 'coherent'.

5.1. *Interpretation in terms of incoherent scatter*

The most obvious assumption made in deriving equation (10), and hence in determining the expected gain values h presented in Fig. 15, is that there is no increase in plasma density N_e accompanying the rise in apparent ion temperature T_{im} from 1000K to 5000K.

5.1.1. *Photochemical plasma density changes.* The large ion drifts required to raise T_i and T_{im} are expected to deplete the F-region plasma by increasing the rate of loss of O^+ ions by interaction with neutral gas molecules (SCHUNK and RAITT, 1980). This is frequently thought to be the cause of F-region depletions in regions of high plasma drift (EVANS *et al.*, 1983; LOCKWOOD *et al.*, 1984). Hence, N_e is expected to decrease, not increase, with increased T_i, and hence T_{im}, if the effect is due to photochemistry alone.

Furthermore, the changes in scattered power are too rapid to be satisfactorily explained by production and loss mechanisms. For the example discussed previously, namely gate 3 during 08 : 13–08 : 23 UT on 25 August 1985, Fig. 15(b) shows that 3.5 dB more power is observed than predicted by equation (10). The average density deduced by the standard analysis procedure $\langle N_{em}\rangle$ for the period 08 : 19–08 : 23 UT (when T_{im} and P have returned to steady values and the spectra have typical F-region, twin-peaked forms; see Figs. 6 and 7) is $1.19 \cdot 10^{10}\,m^{-3}$. After the period of exceptionally high power beginning at 08 : 13 : 00 UT, N_{em} fell to near this 'base level' value, being $0.98 \cdot 10^{10}\,m^{-3}$ at 08 : 15 : 45 UT, having been $2.38 \cdot 10^{10}\,m^{-3}$ just 90 s earlier at 08 : 14 : 15 UT. Thus, for the standard analysis procedure to be correct a fall in densities of $\Delta N_e = \Delta N_{em}$ of $1.4 \cdot 10^{10}\,m^{-3}$ must have occurred in $\Delta t = 90\,s$. For this to be *in situ* losses requires a loss rate coefficient (assuming a linear loss law applicable to these observations close to the $F2$-peak) $\beta \approx [(\Delta N_e/\Delta t)/\langle N_e\rangle] > 10^{-2}\,s^{-1}$ (minimum value applicable to zero production rate). This is two orders of magnitude larger than that typically expected for the $F2$-peak. Hence the changes in scattered power cannot be ascribed to a photochemical loss mechanism. Similar arguments can be applied to periods of increasing power and it is found that the rate of change is too rapid to be ascribed to particle or photoionization production rates.

5.1.2. *Plasma density changes due to plasma transport.* For changes in the plasma density within the scattering volume to be caused by plasma transport, there must be a gradient in the plasma density in the direction of the ion drift v_i (denoted here as the x direction and assumed to be field perpendicular). The transport term in the continuity equation then reduces to $(v_i \cdot dN_e/dx)$. For v_i of $1.5\,km\,s^{-1}$ we would require a gradient (dN_e/dx) of about $10^5\,m^{-4}$ to persist over a distance of 45 km, i.e. N_e must more than double within 45 km. Gradients of this magnitude can exist in the high latitude ionosphere, however, it seems highly unlikely that for all 3 events such a gradient existed at the location of the flow burst immediately before the burst occurred. In addition, for all 3 cases the gradient must have existed for gates 1–3 but not for the higher gates (where the power rise is as predicted for constant N_e). Lastly, we note that for the 27 October event, where v_i (and hence x) is thought to be aligned along the radar look direction, we see no large gradients in N_e from one gate to the next, even allowing for the variation of the altitude with gate number (see fig. 7 of WILLIS *et al.*, 1986).

We conclude that rises in N_e cannot explain the data for 27 October 1984 and that large pre-existing spatial gradients, which are moved over the scattering volume by the zonal component of the flow burst, are possible, but unlikely, explanations of the power rise in the other two events. In addition, the asymmetric spectral forms shown in Figs. 7 and 8 cannot arise from the transport of large pre-existing density gradients alone.

5.1.3. *Line-of-sight currents.* Asymmetric spectra of the kind shown in Figs. 7 and 8 can be produced by large currents along the radar look direction (LAMB, 1962; EVANS, 1969). In such cases the growth of one ion-acoustic peak, due to a reduction of Landau damping, is accompanied by a comparable fall in the other ion-acoustic peak due to increased Landau damping. Hence the net increase in power will be small, if present at all. In addition, the field-perpendicular conductivities of the F-region are normally far too small to allow electron drifts (relative to the ions) of sufficient magnitude at the altitude of these observations (211–350 km, corresponding to gates 1–4). Bursts of very large field-aligned current are expected within the ionospheric signature of flux transfer events (SOUTHWOOD 1987). For $\Phi = 73.5°$ these would give a l-o-s current component, which would be present for all, not just the lower altitude, gates. However, a combination of anomalously high F-region l-o-s current (to give the observed spectral shape) and large density gradients with some residual ion mobility (to give the rise in total power) could explain the observations. Note, however, that the gradients would be required to be even larger than quoted above, as the reduction in ion mobility required to give the l-o-s current will also reduce the bulk plasma drift velocity.

5.1.4. *Velocity shears.* HORNE (1987) has pointed out that asymmetric spectra can readily be produced by superposing two Maxwellian spectra with different Doppler shifts. Hence, a velocity shear with different spatial and/or temporal weighting of the contributions to the total scattered power from the two different velocity populations will produce such spectra. In such cases the total scattered power does not increase more than that predicted for the apparent ion temperature rise. The apparent ion temperature T_{im} is raised by the smearing effect by more than the real rise in T_i due to ion–neutral frictional heating. Hence this effect would tend to give smaller, not larger, h.

5.1.5. *Ion composition changes*. The depletion of F-layer plasma by large ion drifts, as discussed above, occurs because O^+ ions are converted to NO^+ (SCHUNK and RAITT, 1980). Hence, the molecular ion fraction is expected to rise during flow bursts. The analysis employed to derive T_{im} assumes that the plasma is almost 100% O^+ ions for all range gates. The presence of molecular ions would cause T_{im} to be an underestimate of T_i, even for Maxwellian, isotropic plasma. Hence, a rise in the molecular ion fraction during the flow burst could cause higher values of h. If, for example, the plasma was 100% O^+ ions when P was low but pure molecular oxygen ions (O_2^+ being the heaviest F-region molecular species) at the peak P during the flow burst, equation (7) predicts an additional gain of only 0.5 dB for $\alpha = 0.43$ and $T_e = 2112$K (applicable to gate 3 and 08 : 13–08 : 23 UT on 25 August 1985). This is inadequate to explain the 3.5 dB difference between the observed and predicted h (see Fig. 15b), even if such a dramatic composition change were possible on the short time scales of the power fluctuations.

It should be noted that a change in ion composition could produce some variation in the shape of the ion line spectrum when there was a mixture of O^+ and molecular ions, in a manner similar to that predicted by MOORCROFT (1964) for O^+ and lighter ions.

5.1.6. *Changes in* α, F *and* T_{em}. We have also considered how a change in the α value could affect the rise in observed power. From the spectral shape we infer that the real electron temperature T_e has a maximum value of 5000K (greater T_e would give a double humped spectrum for Maxwellian plasma or a triple humped spectrum for non-Maxwellian). By equation (5) this limits the maximum value of α (real value as opposed to that deduced by the incoherent scatter analysis) to ≈ 0.8. If the α value deduced for $T_{im} = 1000$K is assumed to be correct [≈ 0.4; see Fig. 12(a)] this gives a maximum additional gain h [equation (10)] of about 1 dB. As well as being inadequate to explain Fig. 15, such an effect cannot explain the departures from twin-peaked spectra.

In deriving equation (10) it was assumed that T_{em} remains constant. Figure 12(b) demonstrates that a slight decrease in T_{em} is observed with increasing T_{im}, giving values of 2100K and 1700K at T_{im} of 1000K and 5000K, respectively. Equation (10) shows that for this case a mere 0.2 dB of additional gain results from the fall in T_{em} for $F_1 = F_5 = 1$.

Lastly, we must consider changes in F [equation (8)]. The plasma will be nearly thermal when $T_{im} = 1000$K ($\approx T_n$), giving $F_1 = 1$. As discussed previously, we expect $F_5 < 1$ for non-thermal and anisotropic plasma with $\Phi > 54.7°$. By equation (10) this further decreases the predicted h value, and the adoption of $F_5 = 1$ in Fig. 15 gives maxima of predicted h. For example, if F were 0.5, the computed h is roughly 0.5 dB lower than for $F_5 = 1$ [from equation (10)]. There is no F_5 which will give the 3.5 dB required to explain the example of gate 3 during the interval 08 : 13–08 : 23 UT on 25 August 1985; even in the limit of F_5 tending to infinity, the additional gain is only 1 dB.

5.2. *Interpretation in terms of coherent echo contamination of the incoherent scatter ion line*

There have been a number of observations reporting coherent echoes at 'large' ($> 1°$) angles from perpendicularity to the geomagnetic field (MCDIARMID, 1972, 1976; OGAWA *et al.*, 1980; SOFKO *et al.*, 1983). We are aware of only two sets of observations of coherent echoes at an aspect angle greater than the 16.5° employed by U.K.–POLAR: MCDIARMID and MCNAMARA (1969) found echoes at an aspect angle of 20° and E-region echoes at values up to 20° have been detected during storms by the Millstone Hill radar, using a frequency of 440 MHz (ST.-MAURICE *et al.*, 1987). However, it should be noted that the maximum angle at which echoes are observed is a function of the radar power, sensitivity and antenna gain, there being a gradual decrease in power with aspect angle (termed the aspect sensitivity) and no sharp cut-off. Hence, it is to be expected that incoherent power and antenna gains, will be influenced by coherent echoes at much greater aspect angles than coherent systems. In addition, it should be noted that we are dealing with UHF echoes (frequency 933 MHz) from the ionospheric F-region. It is well known that the irregularities causing coherent echoes are not the same in the E- and F-regions (FEJER and KELLY, 1980) and that there are considerable variations with wavelength at any given height. Most of the literature on coherent echoes deals with E-region scatter, although F-region effects have long been known (WEAVER, 1965). Perpendicularity in the F-region is only possible for ground-based radars which use HF wavelengths, by virtue of ionospheric ray path bending of HF signals. OKSMAN *et al.* (1979) have compared E-region coherent VHF echoes with F-region HF backscatter data.

5.2.1. *Radar equations for coherent and incoherent scatter.* In evaluating the possible effect of coherent echoes, we must first consider the nature of the incoherent and coherent scattering process in relation to the radar equation. For a 'soft' target which fills the radar beam, as is the case for incoherent scatter (EVANS, 1969), the radar equation is the same as for coherent scatter from irregularities which fill the scattering volume (FARLEY *et al.*, 1981). It is frequently assumed that the irregularities fill the scattering volume in the azimuthal direction but not in the elevational (ECKLUND *et al.*, 1975). In these cases, a different form of the radar equation applies (WALDOCK *et al.*, 1985; OKSMAN *et al.*, 1986). Here we assume that any irregularities do fill the scattering volume (which is roughly 13 km by 13 km), which requires that they be in a slab which is at least $\Delta h = 13$ km thick. Then we can simply compare the cross sections for coherent and incoherent scatter.

5.2.2. *Volume cross sections for coherent scatter.* Cross sections for F-region scatter at look directions very close to perpendicularity are not known for UHF systems. FARLEY *et al.* (1981) found typical values of $10^{-10}\,m^2\,m^{-3}$ using a 50 MHz radar to study the equatorial E-layer. OKSMAN *et al.* (1986) showed that for another radar of similar frequency (the PGI2 system in the U.S.S.R. which employs 45 MHz) the value is larger and around $2\cdot10^{-9}\,m^2\,m^{-3}$ for auroral E-region scatter. These authors also consider a variety of auroral E-region radars and show that the cross section tends to fall with frequency and is near $10^{-14}\,m^2\,m^{-3}$ for the 400 MHz system in Homer, Alaska. HAGFORS (1971) gives a value near $10^{-12}\,m^2\,m^{-3}$ for the 1295 MHz system at Millstone Hill (a frequency greater than the 933 MHz employed here) for echoes from around 100 km. Similarly, CHESTNUT *et al.* (1971) deduced that the cross section decreases with increasing frequency by a larger factor of about 30 dB between 139 and 1210 MHz. These authors deduced a wavelength-cubed dependence, consistent with the observations by OKSMAN *et al.* (1979).

5.2.3. *Aspect sensitivity of coherent scatter.* If we adopt a typical E-region value for the peak backscatter volume cross section of $10^{-12}\,m^2\,m^{-3}$ and take an incoherent scatter volume cross section of $N_e\sigma_e \approx 10^{-18}\,m^2\,m^{-3}$ ($N_e \approx 10^{10}\,m^{-3}$) we have, for a hypothetical look direction parallel to B, a ratio of coherent to incoherent scattered powers of 10^6 (i.e. 60 dB). Hence, to get coherent echoes at the aspect angle of U.K.–POLAR (16.5°), which have roughly one-third of the power of incoherent scatter echoes [≈ 5 dB down; see Fig. 6(a)], requires an average aspect sensitivity $< 65/16.5 \approx 4$ dB per degree. There is considerable variety in the values of aspect sensitivity reported in the literature: some UHF, E-region values near zero have been reported (see review by MOORCROFT, 1985), whereas more typical values are around 10 dB per degree (KOEHLER *et al.*, 1985). WALDOCK *et al.* (1985) have found values between 0 and 10 dB and shown that the aspect sensitivity correlates well with the peak backscattered power. This raises the possibility that the power falls rapidly at small aspect angles, close to perpendicularity, but is less aspect sensitive at greater aspect angles, as was suggested by MCDIARMID (1976).

The additional power deduced here is for F-region gates if it is received in the main beam of the antenna (note that gate 1 is centred on 211 km altitude, but has some contributions from heights down to about 180 km). Hence, although the above discussion indicates that coherent echoes comparable to incoherent echoes for the aspect angle of U.K.–POLAR are possible for typical observed cross sections and aspect sensitivities reported for E-region scatter, it is not clear that the same will be true at the F-region heights studied by U.K.–POLAR. Very little is known about F-region cross sections and aspect sensitivities and what has been evaluated is mainly for HF systems. We note an aspect sensitivity of 5 dB per degree has been reported for F-region HF backscatter by BATES and ALBEE (1970), consistent with what is required here if the F-region cross section is comparable to that for the E-region. TAYLOR (1971) has modelled the effects of non-specular clutter from 10 m, F-region density irregularities on incoherent scatter signals. He concluded that such effects are not usually a problem at wavelengths below 4 m. However, at high latitudes this is not the case if the autocorrelation function describing the irregularities becomes non-Gaussian, such as may occur in 'radio star fades'. In addition, highly transient phenomena could possibly give transient non-specular echoes. Wave packets of limited extent both parallel and perpendicular to the geomagnetic field may also explain large aspect angle echoes, and short-lived secondary irregularities may produce these (MOORCROFT, 1984).

5.2.4. *Signals received in antenna sidelobes.* The measured directional gain pattern of the EISCAT UHF antenna at Tromsø, $G'(\gamma)$, where γ is the angle with respect to the direction of the peak antenna gain and G' is measured relative to that peak gain, is described in EISCAT Report 78/7 (1978). At $\gamma > 2°$, G' is everywhere less than -35 dB, and the maxima of the G' fluctuations fall approximately linearly to -60 dB over the range $\gamma = 2$–$85°$. The main secondary maximum of G' (the main sidelobe) is at $\gamma = 88°$, where $G' = -45$ dB.

For a given range gate it is possible that signals are received from either the *E*- or the *F*-regions, via these sidelobes, at different elevations. However, these directions are further from perpendicularity to the geomagnetic field than the main beam for the U.K.–POLAR look direction. This, along with the much lower antenna gain, indicates that coherent echoes received at $\gamma > 2°$ are unlikely.

The spectra indicate that the additional power is at a frequency which is not equal to the mean Doppler shift of the ion line spectrum (that due to l-o-s bulk plasma flow). This could be explained as sidelobe reception of signals scattered from a region of different plasma flow to that in the main beam at the same range. The frequency of the additional power is close to the *F*-region ion-acoustic frequency and this eliminates the possibility of *E*-region echoes, which have been found to be limited to the lower *E*-region ion-acoustic frequency (NIELSEN and SCHLEGEL, 1983). Even if the 'saturation' effect did not occur, or if the echoes were received from the *F*-region via the sidelobe, the flow velocity would have to be unrealistically large to give such a large Doppler shift.

Lastly, we note that sidelobe reception calls for much greater spatial scales of flow bursts than have previously been considered. The second beam direction used in the 27 October 1984 experiment is found to lie close to the edge of the event (TODD *et al.*, 1986) and interpretation in terms of a flux transfer event also limits the spatial extent of the flow burst to several hundred kilometers. Hence, these events should not extend to the range gates of the sidelobe beams and we would not expect simultaneous changes in the main beam and sidelobe signals.

All these considerations indicate that the additional power is not received via the antenna sidelobes, but is in the main beam ($\gamma < 2°$) and hence originated from the lower *F*-region.

5.2.5. *Possible scattering waves.* The spectra indicate that the additional power is added at the downshifted ion-acoustic frequency. It is now well established that *E*-region coherent echoes have a limiting Doppler shift at the ion-acoustic speed (NIELSEN and SCHLEGEL, 1983; ROBINSON, 1986). MOORCROFT (1984) has pointed out that the two-stream instability in the *E*-region should result in coherent echo spectra with asymmetric peaks near the ion-acoustic frequency, as has been observed by HOFSTEE and FORSYTH (1972), MOORCROFT and TSUNODA (1977) and MOORCROFT and RUOHONIEMI (1987). For the *F*-region the possible sources of ion-acoustic waves above the background thermal fluctuation level (that detected by incoherent scatter) is unclear, as is the reason for their apparent propagation in a plane well removed from the preferred field-perpendicular plane. It is possible that such waves may be generated directly by the large plasma drifts (in the presence of weak ion–neutral collisions), which also generate the non-thermal ion velocity distributions seen during these periods and at greater altitudes. Alternatively, the waves may be driven by the non-thermal distributions themselves. OTT and FARLEY (1975) and ST.-MAURICE (1978) have predicted that the Post–Rosenbluth instability (ROSENBLUTH and POST, 1965) is the lowest threshold instability to appear in this way. Mechanisms for non-linear mode coupling with ion-acoustic waves could be one possible explanation of our data.

However, there is one major problem with the above ideas. Any instability in the *F*-region is excited in the plasma frame of reference and must drift with the plasma at *F*-region altitudes. Hence, if there were an *F*-region saturation effect at the ion-acoustic frequency, it would occur in the frame of the drifting plasma and would produce two symmetric peaks about the mean Doppler shift. This is consistent with observations suggesting that the irregularities which give *F*-region HF backscatter drift with the bulk plasma flow, as deduced from comparisons of data from SAFARI and EISCAT (VILLAIN *et al.*, 1985) and Goose Bay and Sondrestrom (RUOHONIEMI *et al.*, 1987) radars.

Hence, there is a problem in explaining the asymmetry of the spectra. This could be due to the peak excitation being a few degrees off perpendicularity to the geomagnetic field, i.e. there is a non-zero parallel wave vector. In this case the up- and down-going waves give different scattering cross sections and one peak is stronger than the other in the received spectrum.

Another candidate for generating coherent-like echoes is asymmetric Doppler-shifted ion-cyclotron emissions. These have been reported in the lower *F*-region by coherent radars (FEJER *et al.*, 1984) and by rocket soundings (OGAWA, 1987). These emissions are driven by very large field-aligned currents of the kind expected in association with the twin vortex flow signature of flux transfer events (SOUTHWOOD, 1987).

5.2.6. *Consequences for incoherent scatter.* Finally, it should be noted that the possibility of coherent echo contamination of low elevation signals has very serious consequences for interpretation of EISCAT data, including that from the more northerly beam directions of CP-3-E. The most obvious consequence is that the plasma density will be overestimated and temperatures will be in error (in addition to the errors introduced by the presence of the non-thermal plasma). In addition, plasma velocities may be corrupted as the coherent echo appears to be centred on the ion-acoustic speed, not on the bulk flow velocity of the remaining incoherent ion line spectrum. However, we note that Fig. 5 shows no velocity fluctuations in phase with the power oscillations seen in Fig. 6. We conclude that any coherent echoes must be a sufficiently small fraction of the incoherent signal to make any effect on the velocities negligible for at least the events presented in this paper.

6. CONCLUSIONS

The power scattered from altitudes above about 300 km during very rapid flow bursts rises by an amount predicted by numerical simulations of incoherent scattering from a non-thermal plasma. Non-thermal plasmas are identified by the characteristic spectral shape, a rise in apparent ion temperature T_{im} (deduced by assuming a Maxwellian l-o-s ion velocity distribution) which is too great to be consistent with a bi-Maxwellian ion velocity distribution and an anti-correlation of apparent electron and ion temperatures T_{em} and T_{im}. The rise in power for non-thermal plasma has been found numerically to be within a few per cent of that for a Maxwellian plasma of the same electron temperature and true, 3-dimensional ion temperature.

The power scattered from *F*-region altitudes below about 300 km, however, reveals increases which are larger than predicted, by up to about 6 dB. The additional power rises monotonically with decreasing altitude and is shown to be transient, coming in bursts lasting less than one 15 s integration period (Fig. 6a) and at a frequency close to the downshifted ion-acoustic frequency (i.e. the wave travelling in the same direction as the plasma drift). Various explanations of this additional power in terms of incoherent echoes from non-thermal or thermal plasma are unsatisfactory in that they require the occurrence of what we feel are an unlikely set of circumstances, the least unlikely being large density gradients along the flow direction accompanied by large l-o-s currents. For one example (27 October 1984) we are able to show that the large spatial density gradient required is present neither immediately before nor after the flow burst event. In addition, density gradients alone do not explain the form of the received spectra.

The theory of *F*-region UHF backscatter echoes is not developed sufficiently to predict what power of coherent echo could be expected for the very large aspect angle of 16.5° employed by U.K.–POLAR. It is a matter of some urgency to investigate this possibility further from the point of view of the incoherent scatter technique.

Acknowledgements—We thank the director and staff of EISCAT for their help. EISCAT is supported by the British SERC, French CNRS, West German MPG, Norwegian NAVF, Swedish NFR and Finnish SA. K. S. is supported by the Oskari Huttunen Foundation of Finland with assistance from an ORS scholarship and the Academy of Finland. The work of J.-P. ST.-M. and K. K. was funded by NSF (U.S.A.) grant ATM 8400929 and H. T. is supported by an SERC studentship. The authors are grateful to H. RISHBETH for his comments on this manuscript.

REFERENCES

BARAKAT A. R., SCHUNK R. W. and ST.-MAURICE J.-P. 1983 *J. geophys. Res.* **88,** 3237.
BATES H. F. and ALBEE P. R. 1970 *J. geophys. Res.* **75,** 165.
BEYNON W. J. G. and WILLIAMS P. J. S. 1978 *Rep. Prog. Phys.* **41,** 909.
BUNEMAN O. 1962 *J. geophys. Res.* **67,** 2050.
CHESTNUT W. G., HODGES J. C. and LEADABRAND R. L. 1971 Final report SRI project number 6548, SRI, Menlo Park, California, U. S.A.
ECKLUND W. L., BALSLEY B. B. and GREENWALD R. A. 1975 *J. geophys. Res.* **80,** 1805.
EVANS J. V. 1969 *Proc. IEEE* **57,** 496.
EVANS, J. V., HOLT J. M., OLIVER W. L. and WAND, R. H. 1983 *J. geophys. Res.* **88,** 7769.
FARLEY D. T., IERKIC H. M. and FEJER B. G. 1981 *J. geophys. Res.* **86,** 1569.
FARMER A. D., LOCKWOOD M., FULLER-ROWELL T. J. and LØVHAUG, U. P. 1988 *J. atmos. terr. Phys.* **50,** 487.
FEJER B. J. and KELLEY M. C. 1980 *Rev. Geophys. Space Phys.* **18,** 401
FEJER B. J., REED R. W., FARLEY D. T., SWARTZ W. E. and KELLEY M. C. 1984 *J. geophys. Res.* **89,** 187.
HAGFORS T. 1971 Paper number 9, AGARD Conference Proceedings 97.
HOFSTEE J. and FORSYTH P. A. 1972 *J. atmos. terr. Phys.* **34,** 893.
KOEHLER J. A., SOFKO G. J. and METHA V. 1985 *Radio Sci.* **20,** 689.
HUBERT D. 1984 *J. atmos. terr. Phys.* **46,** 601.
LAMB G. L. 1962 Los Alamos Science Laboratory, Report LA2715.
LOCKWOOD M. and FULLER-ROWELL T. J. 1987A *Geophys. Res. Lett.* **14,** 371.
LOCKWOOD M. and FULLER-ROWELL T. J. 1987B *Geophys. Res. Lett.* **14,** 581.

LOCKWOOD, M., BROMAGE B. J. I., HORNE R. B., ST.-MAURICE J.-P., WILLIS D. M. and COWLEY S. W. H. 1987 *Geophys. Res. Lett.* **14**, 111.
LOCKWOOD M., FARMER A. D., OPGENOORTH H. J. and CROTHERS S. R. 1984 *J. atmos. terr. Phys.* **46**, 489
LOCKWOOD M., VAN EYKEN A. P., BROMAGE B. J. I., WILLIS D. M. and COWLEY S. W. H. 1986A *Geophys. Res. Lett.* **13**, 72.
LOCKWOOD M., VAN EYKEN A. P., BROMAGE B. J. I., WAITE J. H. JR, MOORE T. E. and DOUPNIK J. R. 1986B *Adv. Space Res.* **6**, 93.
MCDIARMID D. R. 1972 *Can. J. Phys.* **50**, 2557.
MCDIARMID D. R. 1976 *J. geophys. Res.* **81**, 4007.
MCDIARMID D. R. and MCNAMARA A. G. 1969 *Can. J. Phys.* **47**, 1271.
MOORCROFT D. 1963 *J. geophys. Res.* **68**, 4870.
MOORCROFT D. 1964 *J. geophys. Res.* **69**, 955.
MOORCROFT D. 1984 *J. geophys. Res.* **98**, 2963.
MOORCROFT D. 1985 *Can. J. Phys.* **63**, 1005.
MOORCROFT D. and RUOHONIEMI J. M. 1987 J. geophys. Res. **92**, 3333.
MOORCROFT D. and SCHLEGEL K. 1988 *J. atmos. terr. Phys.* **50**, 455.
MOORCROFT D. and TSUNODA R. T. 1977 *J. geophys. Res.* **83**, 1482.
NIELSEN E. and SCHLEGEL K. 1983 *J. geophys. Res.* **88**, 5745.
OGAWA T., BALSLEY B. B., ECKLAND W. L., CARTER D. A. and JOHNSTON P. E. 1980 *Geophys. Res. Lett.* **7**, 1081.
OKSMAN J., MOLLER H. G. and GREENWALD R. A. 1979 *Radio Sci.* **14**, 1121.
OKSMAN J., USPENSKY M. V., STARKOV G. V., STEPANOV G. S. and VALLINKOSKI M. 1986 *J. atmos. terr. Phys.* **48**, 107.
OTT E. and FARLEY D. T. 1975 *J. geophys. Res.* **80**, 4599.
RAMAN R. S. V., ST.-MAURICE J.-P. and ONG, R. S. B. 1981 *J. geophys. Res.* **86**, 4751.
ROBINSON T. R. 1986 *J. atmos. terr. Phys.* **48**, 417.
ROSENBLUTH M. N. and POST R. F. 1965 *Phys. Fluids* **8**, 547.
RUOHONIEMI J. M., GREENWALD R. A., BAKER K. B., VILLAIN J. P. and MCCREADY M. A. 1987 *J. geophys. Res.* **42**, 4553.
SCHUNK R. W. and RAITT W. J. 1980 *J. geophys. Res.* **85**, 1255.
SOFKO G. J., KOEHLER J. A., GILMER J., MCNAMARA A. G. and MCDIARMID D. R. 1983 *Adv. Space Res.* **2**, 149.
ST.-MAURICE J.-P. 1978 *Planet. Space Sci.* **26**, 801
ST.-MAURICE J.-P. 1987 *J. geophys. Res.* **92**, 4533.
ST.-MAURICE J.-P. and HANSON W. B. 1982 *J. geophys. Res.* **87**, 7580.
ST.-MAURICE J.-P. and SCHUNK R. W. 1979 *Rev. Geophys. Space Sci.* **17**, 99.
ST.-MAURICE J.-P., HANSON W. B. and WALKER J. C. G. 1976 *J. geophys. Res.* **81**, 5438.
SOUTHWOOD D. J. 1987 *J. geophys. Res.* **92**, 3207.
SUVANTO K. 1987 *Planet. space Sci.* **35**, 1429.
TAYLOR G. N. 1971 Paper number 13, AGARD Conference Proceedings 97.
TODD H., BROMAGE B. J. I., COWLEY S. W. H., LOCKWOOD M., VAN EYKEN A. P. and WILLIS D. M. 1986 *Geophys. Res. Lett.* **13**, 909.
TODD H., COWLEY S. W. H., ETAMADI A., BROMAGE B. J. I., LOCKWOOD M., WILLIS D. M and LÜHR H. 1988 *J. atmos. terr. Phys.* **50**, 423.
VAN EYKEN A. P., RISHBETH H., WILLIS D. M. and COWLEY S. W. H. 1984 *J. atmos. terr. Phys.* **46**, 635.
VILLAIN J. P., CLAUDEL G. and HANUISE C. 1985 *J. geophys Res.* **90**, 8433.
WALDOCK J. A., JONES T. B., and NIESLON E. 1985 *Radio Sci.* **20**, 709.
WEAVER P. F. 1965 *J. geophys. Res.* **70**, 5425.
WILLIS, D. M., LOCKWOOD M., COWLEY S. W. H., VAN EYKEN A. P., BROMAGE B. J. I., RISHBETH H., SMITH P. R. and CROTHERS S. R. 1986 *J. atmos. terr. Phys.* **48**, 987.
WINSER K. J., LOCKWOOD M. and JONES G. O. L. 1987 *Geophys. Res. Lett.* **14**, 957.

Reference is also made to the following unpublished material:
BUCHERT S. 1987 Private communication.
HORNE R. B. 1987 Private communication.
HUBERT D. 1987 Private communication.
MOORCROFT D. 1987 Private communication.
OGAWA T. 1987 Private communication.
ST.-MAURICE J.-P. 1987 Unpublished manuscript.